Kwon et al. *NPG Asia Materials* (2020) 12:86
https://doi.org/10.1038/s41427-020-00270-z

NPG Asia Materials

ARTICLE Open Access

High-density Néel-type magnetic skyrmion phase stabilized at high temperature

Hee Young Kwon[1], Kyung Mee Song[1], Juyoung Jeong[2,3], Ah-Yeon Lee[4], Seung-Young Park[5], Jeehoon Kim[2,6], Changyeon Won[7], Byoung-Chul Min[1,8], Hye Jung Chang[3,8] and Jun Woo Choi[1]

Abstract

The discovery of a thermally stable, high-density magnetic skyrmion phase is a key prerequisite for realizing practical skyrmionic memory devices. In contrast to the typical low-density Néel-type skyrmions observed in technologically viable multilayer systems, with Lorentz transmission electron microscopy, we report the discovery of a high-density homochiral Néel-type skyrmion phase in magnetic multilayer structures that is stable at high temperatures up to 733 K (≈460 °C). Micromagnetic simulations reveal that a high-density skyrmion phase can be stabilized at high temperature by deliberately tuning the magnetic anisotropy, magnetic field, and temperature. The existence of the high-density skyrmion phase in a magnetic multilayer system raises the possibility of incorporating chiral Néel-type skyrmions in ultrahigh-density spin memory devices. Moreover, the existence of this phase at high temperature shows its thermal stability, demonstrating the potential for skyrmion devices operating in thermally challenging modern electronic chips.

Introduction

Skyrmions in magnetic materials have been extensively studied due to their nontrivial topology; this topology leads to many interesting fundamental and dynamical properties[1–3]. The nanometer size and efficient current-driven manipulation of skyrmions make them suitable for high-density, low-power spin memory devices[1–10]. Magnetic skyrmions have been observed in various material systems that experience Dzyaloshinskii–Moriya interaction (DMI) due to broken inversion symmetry, such as noncentrosymmetric single crystals[1,2,4,5], ultrathin epitaxial systems[3,6], and magnetic multilayers[10–15]. Skyrmions in magnetic multilayers, which possess homochiral Néel domain walls, have two main advantages in application compared to those in other material systems: (1) they are stabilized at room temperature[10–15] and (2) they exhibit current driven unidirectional translation motion[12,16–18]. This motion is due to the electric current induced spin-orbit torque (SOT) acting on the homochiral Néel domain walls of the magnetic multilayer skyrmions; the SOT exerts a unidirectional force on the homochiral Néel domain walls, causing the skyrmions to move with or against the electric current direction depending on the chirality of the system[19]. This is not the case for magnetic skyrmions with Bloch domain walls (e.g., skyrmions in complex noncentrosymmetric systems such as B20 structures) or magnetic bubbles with mixed chirality. In fact, in magnetic multilayer systems, various SOT-induced skyrmion dynamics such as skyrmion creation[6,10,16,17,20–22], annihilation[6,10,20], gyration[23], and breathing-like motion[24] have been experimentally demonstrated. These current driven dynamics occurring on the nanosecond time scale in room-temperature Néel-type skyrmions raise the possibility of their potential application in spin memory and spin logic devices.

One unresolved issue that needs to be overcome for practical applications of Néel-type multilayer skyrmions is their low density. Skyrmion lattice structures are not found. Typically, in multilayers, isolated skyrmions in a background

Correspondence: Hye Jung Chang (almacore@kist.re.kr) or Jun Woo Choi (junwoo@kist.re.kr)
[1]Center for Spintronics, Korea Institute of Science and Technology, Seoul 02792, Republic of Korea
[2]Department of Physics, Pohang University of Science and Technology, Pohang 37673, Republic of Korea
Full list of author information is available at the end of the article
These authors contributed equally: Hee Young Kwon, Kyung Mee Song, Juyoung Jeong

of uniform magnetization (distance between skyrmions » skyrmion size) are formed within a narrow range of magnetic fields; when an out-of-plane magnetic field is applied to the stripe phase of the magnetic multilayer system, the stripes break up into isolated skyrmions, eventually becoming a uniform magnetization phase when the magnetic field is further increased[10–15]. Therefore, it is not clear whether the skyrmion phase in multilayers is the true ground state magnetic domain phase or merely a metastable state that appears during the stripe-to-uniform phase change process. Moreover, while isolated, metastable skyrmions are advantageous for skyrmion creation and annihilation and ideal for understanding the mechanisms of skyrmion dynamics excluding any skyrmion–skyrmion interactions, they are significantly disadvantageous in terms of information storage density when utilized in skyrmion-based memory and computing devices. In particular, a high-density skyrmion phase is instrumental for the realization and optimization of theoretically proposed unconventional skyrmion-based computing models (e.g., probabilistic computing, reservoir computing)[25–27]. Note that although there is a report on skyrmion lattices observed in magnetic multilayers[28], isolated skyrmions have been the norm in most magnetic multilayer systems, raising questions about the widespread application of multilayer-based ultrahigh-density skyrmion memory and computing devices.

In this study, using Lorentz transmission electron microscopy (LTEM), we discover a high-density homochiral Néel-type skyrmion phase in a magnetic multilayer system that is stable in a wide temperature range, even at high temperatures above 700 K. Micromagnetic simulations confirm the experimental observations, showing that a high-density Néel-type skyrmion phase can be stabilized by appropriately tuning the temperature-dependent material parameters (e.g., magnetic anisotropy and magnetization). The existence of a high-density skyrmion phase at high temperature demonstrates the thermal stability of this magnetic domain phase. It also suggests that multilayer Néel-type skyrmions could be utilized in nonvolatile spin-based electronic devices that require operation at elevated temperatures (e.g., automotive or military applications)[29]. Our findings can provide an important technological basis for more extensive employment of spin memory devices.

Materials and methods

Growth of the multilayer films

The Ta (3)/Pt (3)/[Pt (0.6)/Co (1.3)/Ru (0.85)/Pt (0.6)/$Co_4Fe_4B_2$ (0.8)/Ru (0.85)]$_{10}$/MgO (2)/Ta (2) films (Fig. 1a; the film thicknesses are given in nanometers; the films are hereafter referred as Pt/Co/Ru/Pt/CoFeB/Ru multilayers) are grown on 100-nm-thick Si_3N_4 membranes and on thermally oxidized Si substrates by DC magnetron sputtering at room temperature in a vacuum chamber with base pressure of $\sim 2 \times 10^{-8}$ Torr.

Magnetic property measurements

The temperature-dependent (400–700 K) material constants (anisotropy field and net saturation magnetization) are determined by vibrating-sample magnetometry (VSM) and superconducting quantum interference device (SQUID) measurements on films grown on a thermally oxidized Si substrate. The magnetic domain structures are observed by LTEM (FEI, Titan 80–300). For LTEM measurements, the films are directly grown on TEM grids with 20-nm-thick Si_3N_4 membranes. The samples are directly heated in TEM using an in situ-heating TEM holder (Gatan Model 652). The Néel wall magnetic domains are visualized in the LTEM after tilting the sample 30° from the film normal direction.

Monte-Carlo simulations

Micromagnetic simulations are performed using the Monte Carlo method with a square grid system and the Heisenberg model, which has been used in many studies to investigate magnetic domains[30,31]. The Hamiltonian used in the simulation is

$$\begin{aligned} H = & -J \sum_{<i,j>} \vec{S}_i \cdot \vec{S}_j - \sum_{<i,j>} \overrightarrow{DM}_{ij} \cdot (\vec{S}_i \times \vec{S}_j) \\ & -K_{\text{eff}} \sum_i \left|\vec{S}_{i,z}\right|^2 + D_{\text{dip}} \sum_{i,j} \frac{\vec{S}_i \cdot \vec{S}_j}{\left|\vec{r}_{ij}\right|^3} - \vec{h}_{\text{ext}} \cdot \sum_i \vec{S}_i \end{aligned}, \quad (1)$$

where J, $\overrightarrow{DM}_{ij}$, $K_{\text{eff}}\left(= K_z - 2\pi M_s^2\right)$, D_{dip}, and $\vec{h}_{\text{ext}}$ are the exchange interaction, DMI, effective perpendicular magnetic anisotropy, magnetic dipole interaction, and external magnetic field, respectively. The other term in the dipole interaction, $-\sum_{i,j} \frac{3(\vec{S}_i \cdot \vec{r}_{ij})(\vec{S}_j \cdot \vec{r}_{ij})}{\left|\vec{r}_{ij}\right|^5}$, mainly contributes to the form of the shape anisotropy[30–32], which is included in the effective perpendicular magnetic anisotropy K_{eff} in Eq. (1). To simplify the calculations, in our model, the spin on a grid site $\vec{S}$ is set as a unit vector, and the $\vec{r}_{ij}$ in the dipole interaction is set as a dimensionless displacement vector, so the Hamiltonian parameters J, $\overrightarrow{DM}_{ij}$, D_{dip}, K_{eff}, and $\vec{h}_{\text{ext}}$ have units of energy. The relations used in our Monte Carlo simulation process to obtain the spin configurations are given as[31,33]

$$\begin{aligned} \left|\vec{S}_{//\,\vec{h}_{\text{eff}}}\right| &= \frac{T \log[\exp(-|\vec{h}_{\text{eff}}|/T) + 2R \times \sinh(|\vec{h}_{\text{eff}}|/T)]}{|\vec{h}_{\text{eff}}|} \\ \left|\vec{S}_{\perp \vec{h}_{\text{eff}}}\right| &= \sqrt{1 - \left|\vec{S}_{//\,\vec{h}_{\text{eff}}}\right|^2} \end{aligned}, \quad (2)$$

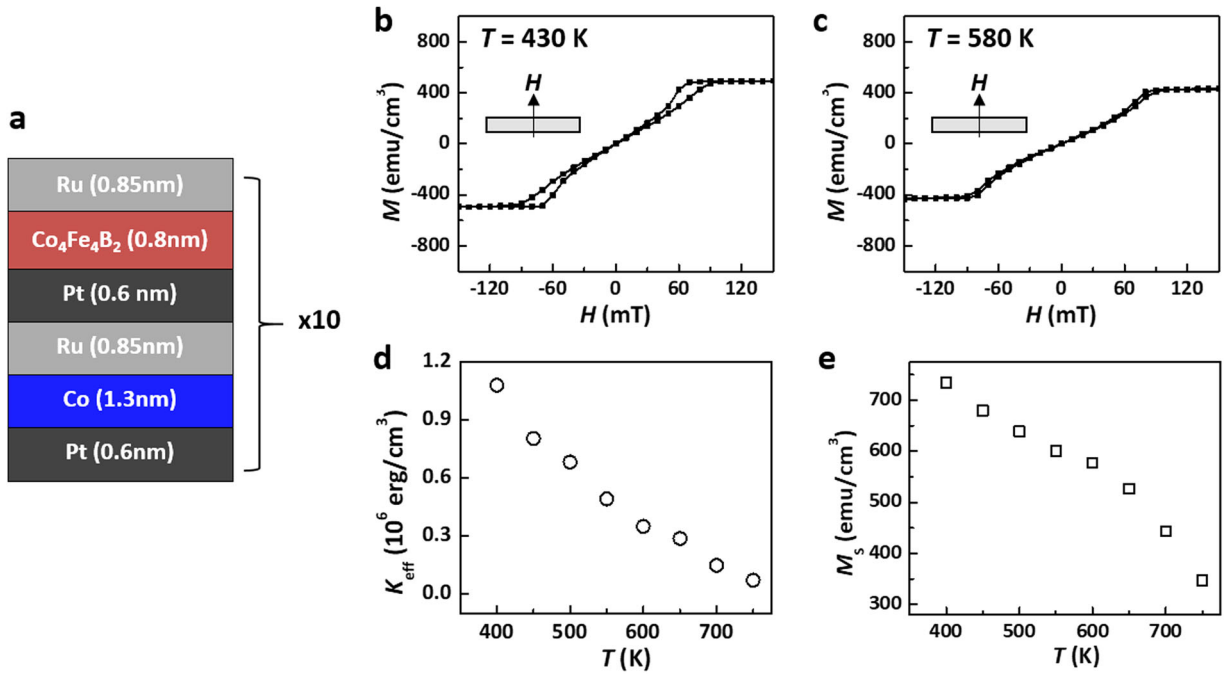

Fig. 1 Magnetic properties of the multilayer samples. a The magnetic multilayer part of the measured sample. **b**, **c** Out-of-plane magnetic hysteresis loops measured by vibrating sample magnetometry (VSM). Representative loops measured at $T = 430$ K (**b**) and $T = 580$ K (**c**). **d**, **e** Temperature dependence of the effective magnetic anisotropy K_{eff} (**d**) and the saturation magnetization M_s (**e**). M_s and K_{eff} ($= H_k \times M_s/2$), where H_k is the anisotropy field, obtained by measuring the temperature-dependent hard axis (in-plane) magnetic hysteresis loops (see SI Fig. S3).

where R is a random number, T is the temperature parameter, and $\vec{h}_{\text{eff}}$ $(\equiv \frac{1}{\mu_0}\frac{\partial H}{\partial \vec{S}_i})$ is the effective field. $\vec{S}_{//\vec{h}_{\text{eff}}}$ and $\vec{s}_{\perp\vec{h}_{\text{eff}}}$ are spin components parallel and perpendicular to $\vec{h}_{\text{eff}}$, respectively. A nonzero temperature T causes the spin directions to deviate from the applied effective field directions, so the various effects caused by the thermal fluctuation of spin vectors can be implemented using these relations in the ensemble average limit.

Results and discussion

Temperature dependence of the magnetic material parameters

Out-of-plane magnetic hysteresis loops of the Pt/Co/Ru/Pt/CoFeB/Ru multilayers (structure shown in Fig. 1a) were measured at high temperature, with representative loops shown in Fig. 1b, c. While the unit layers of Pt/Co/Ru and Pt/CoFeB/Ru have out-of-plane magnetic easy axes (see Supplementary Information (SI) Fig. S1), the Pt/Co/Ru/Pt/CoFeB/Ru multilayer films have near-zero remanent magnetization. We later confirm with LTEM measurements that this is due to the formation of out-of-plane stripe domains with 50:50 up:down magnetization regions. Note that the 0.6-nm-thick Pt layers adjacent to the CoFeB and Co should be fully magnetized due to the magnetic proximity effect[34,35]. Additionally, while the 0.85-nm-thick Ru layer normally induces antiferromagnetic interlayer coupling between adjacent magnetic layers at room temperature[36], above 400 K, the Ru interlayer coupling becomes ferromagnetic due to the annealing effect (see SI Fig. S2), so the full Pt/Co/Ru/Pt/CoFeB/Ru multilayer behaves as a single magnetic layer. The antiferromagnetic-to-ferromagnetic coupling transition is permanent and irreversible; i.e., after the initial temperature increase reaches above 400 K, ferromagnetic coupling remains even when the temperature is decreased back to room temperature. In the process of increasing the temperature from 400 to 750 K, the saturation magnetization M_s and the effective magnetic anisotropy K_{eff} significantly decrease (Fig. 1d, e; the values are obtained from the temperature-dependent hard axis hysteresis loops in SI Fig. S13); we later show, with the LTEM images and simulation results, that the decrease in these material parameters clearly affects the magnetic domain phase.

Temperature dependence of the magnetic domain phase

The temperature- and magnetic field-dependent magnetic domain phases are observed by LTEM measurements. In the LTEM images, the domain contrast is obtained only after tilting the sample by ~30°, which implies that the domains have Néel walls[37,38]. Further details on the Néel wall LTEM contrast are given in SI Fig. S4 and Note 1. The

domains in this multilayer system are expected to possess homochirality due to the interfacial DMI at the Pt/Co and Pt/CoFeB interfaces, which induce left-handed chirality[12,14,19,24]. Figure 2a shows the magnetic domain evolution during the temperature increase process from room temperature to 733 K under a constant out-of-plane magnetic field of 29 mT. The samples remain in an out-of-plane single domain (Fig. 2a–i) up to ~530 K, above which two phase transitions are observed. First, at 540 K, there is a transition from the single domain to the stripe domain phase (Fig. 2a–ii). When the temperature is further increased, another transition from the stripe domain phase to a high-density multiskyrmion state occurs at 733 K (Fig. 2a–vi). Note that dark/bright contrast always appears on

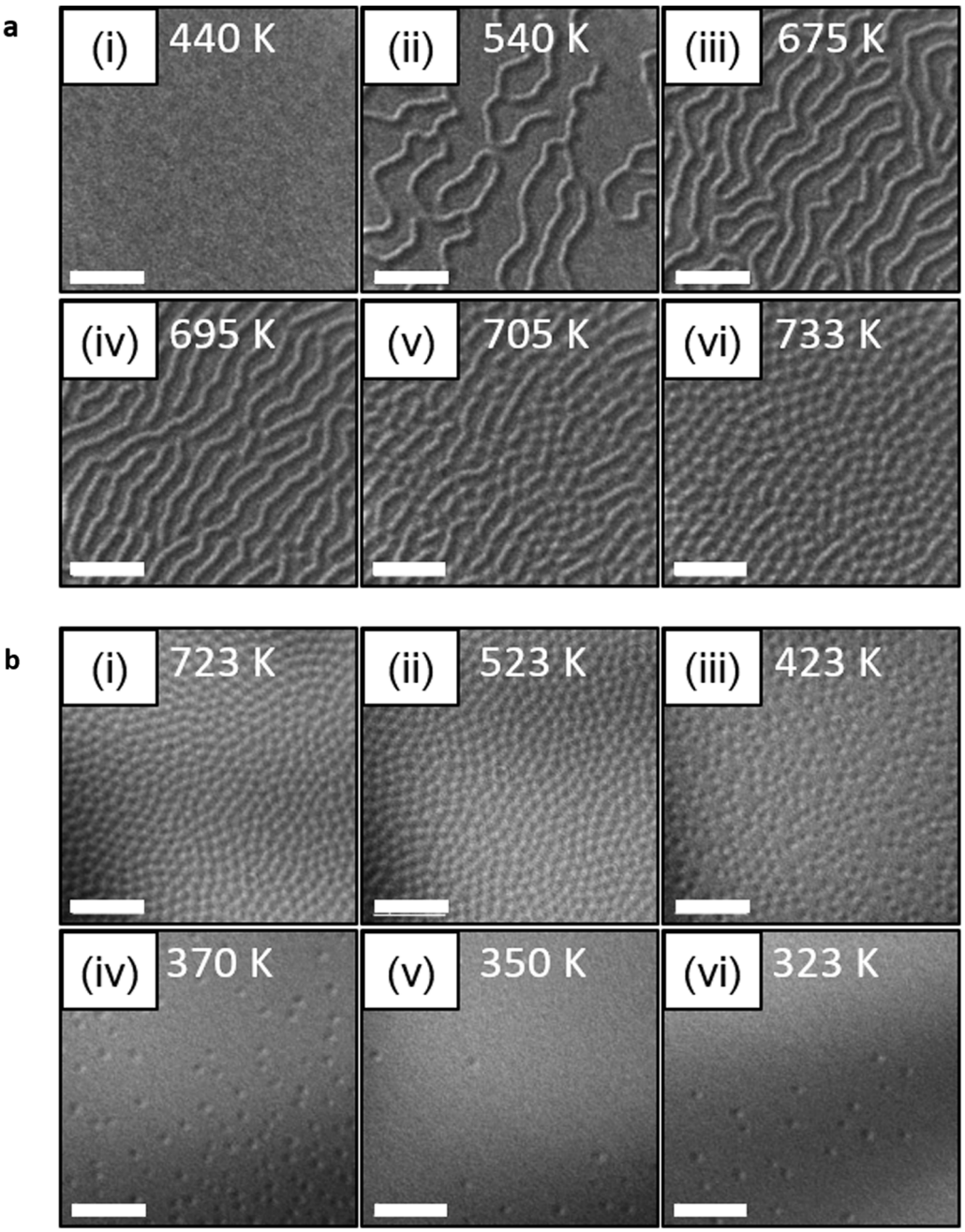

Fig. 2 Temperature-dependent magnetic domain measurements. a, **b** The domain phase evolution of the Pt/Co/Ru/Pt/CoFeB/Ru multilayers observed using Lorentz transmission electron microscopy (LTEM) during the temperature increase (**a**) and decrease (**b**) processes. The LTEM domain contrast is obtained with the sample tilted 30° from the film normal and with a constant out-of-plane magnetic field of $H = 29$ mT. The white scale bars in the images are 1 μm.

the same side of the stripes and skyrmions, indicating that these domains indeed have homochirality[37,38], as discussed earlier (see also SI Note 1). Thus, we observe a high-density homochiral Néel-type skyrmion phase in this multilayer system at significantly high temperatures (>700 K).

As the temperature is decreased back to room temperature, the high-density skyrmion phase remains (Fig. 2b–i and ii) until approximately 423 K, at which point the skyrmion density starts to decrease (Fig. 2b–iii). With a further temperature decrease, the skyrmion density is significantly reduced, and the domains gradually saturate into an out-of-plane single domain (Fig. 2b–iv through vi). During the temperature decrease process, a dense array of skyrmions appears in a wide temperature range of 733–423 K. See SI Fig. S5 for additional LTEM images from the temperature decrease process. Stripe domains do not appear during the temperature decrease in contrast to the temperature increase process, exhibiting a temperature-dependent hysteresis behavior in the magnetic domain phase evolution. At 733 K, the size of the skyrmions is ~155 nm, while the average distance between the skyrmions in the high-density phase is ~195 nm. The methods and accuracies of the skyrmion size and distance measurements are discussed in SI Note 2, Note 3, Figs. S6, and S7. The skyrmion size and distance are roughly unchanged down to 423 K (see SI Fig. S8). Estimation of the skyrmion coverage (the area of skyrmion imprint in a uniform background magnetization) using the skyrmion size and distance is not possible since the measured skyrmions do not form a periodic close-packed (e.g., triangular) lattice. Alternatively, we determine the skyrmion coverage from the out-of-plane hysteresis loops in Fig. 1b, c. For $H = 29$ mT (the out-of-plane field in which the LTEM is measured), the normalized magnetizations ($M_{H=29\mathrm{mT}}/M_\mathrm{s}$) at 430 K and 580 K are 0.275 and 0.237, respectively. This corresponds to coverages of 36% and 38% at 430 K and 580 K, respectively, demonstrating that the homochiral skyrmions observed in Fig. 2a, b do in fact form a high-density phase.

Micromagnetic simulations are performed to reproduce and explain the experimental observations. As discussed earlier, the ferromagnetic coupling between the Co and CoFeB layers ensures that the whole multilayer stack behaves as a single magnetic layer, so the simulations are performed assuming a single two-dimensional (2D) layer. The temperature parameter $T'(\equiv T/J)$ varies during the temperature increase (Fig. 3a) and decrease (Fig. 3b) process at several representative $K'_\mathrm{eff}(\equiv K_\mathrm{eff}/J)$ values. In the simulations, increasing (decreasing) T' has the same effect as decreasing (increasing) M_s since the main origin of the temperature dependence of M_s is the thermal fluctuation (see Methods). The initial state ($T' = 0$ K) in all cases for the temperature increase process is the out-of-plane single domain state due to the presence of an external out-of-plane magnetic field (leftmost images in Fig. 3a), whereas the initial state for the temperature decrease process is the paramagnetic state (rightmost images in Fig. 3b). The experimental observations of the single-stripe-skyrmion domain phase transition during the temperature increase (Fig. 2a) and the decreasing skyrmion density during the temperature decrease (Fig. 2b) are qualitatively reproduced in the simulation results. Considering the temperature dependence of K_eff shown in Fig. 1d, the spin configurations following the direction of the red dotted lines in Fig. 3a, b show phase transition behaviors similar to those observed in experiments. These simulation results clearly indicate that the temperature-dependent change in K_eff significantly contributes to the observed hysteresis behavior, i.e., the different domain phase changes during temperature increase and decrease. In a complementary simulation where $K\prime_\mathrm{eff}$ and T' are simultaneously modulated, the domain evolution in Fig. 2a is once again reproduced (see SI Note 4 and Fig. S9). A recent experimental study reported a large temperature dependence for the DMI[39]. In light of this, we conduct additional simulations with different DMI values. The single-stripe-skyrmion phase transition appears in a wide range of DMI strengths (see SI Note 5 and Fig. S10), suggesting that this domain phase transition could occur even with a large modulation in the DMI.

A more detailed observation of the micromagnetic simulation results during the temperature increase reveals that the appearance of stripe domains depends on the K'_eff values. In the case of low K'_eff (top two rows of Fig. 3a), the out-of-plane single domain transitions into a stripe domain phase and subsequently into a high-density skyrmion phase with increasing temperature. In the case of high K'_eff (bottom row of Fig. 3a), the out-of-plane single domain directly changes into skyrmions without the appearance of stripe domains. Domain nucleation only occurs when the thermal fluctuation can break the uniform magnetization by overcoming an energy barrier proportional to K'_eff; stripe or skyrmion domains are formed when the anisotropy energy scale is similar to the temperature energy scale ($K'_\mathrm{eff} \sim T'$), as shown in Fig. 3a. Hence, at higher K'_eff, the thermal fluctuation is already strong enough to produce small domain structures, i.e., skyrmions, so the stripe phase does not appear in the bottom row of Fig. 3a.

Note that the simulation results in Fig. 3b are obtained sequentially from *right to left* for the temperature decrease process. The initial states are the paramagnetic state, and the temperature is slowly decreased so that the system achieves the magnetic configuration that minimized the energy and entropy. Therefore, Fig. 3b should resemble the ground-state magnetic domain configurations, in which we see skyrmions appearing in a wide temperature range. In the experimentally observed LTEM images during the temperature decrease process

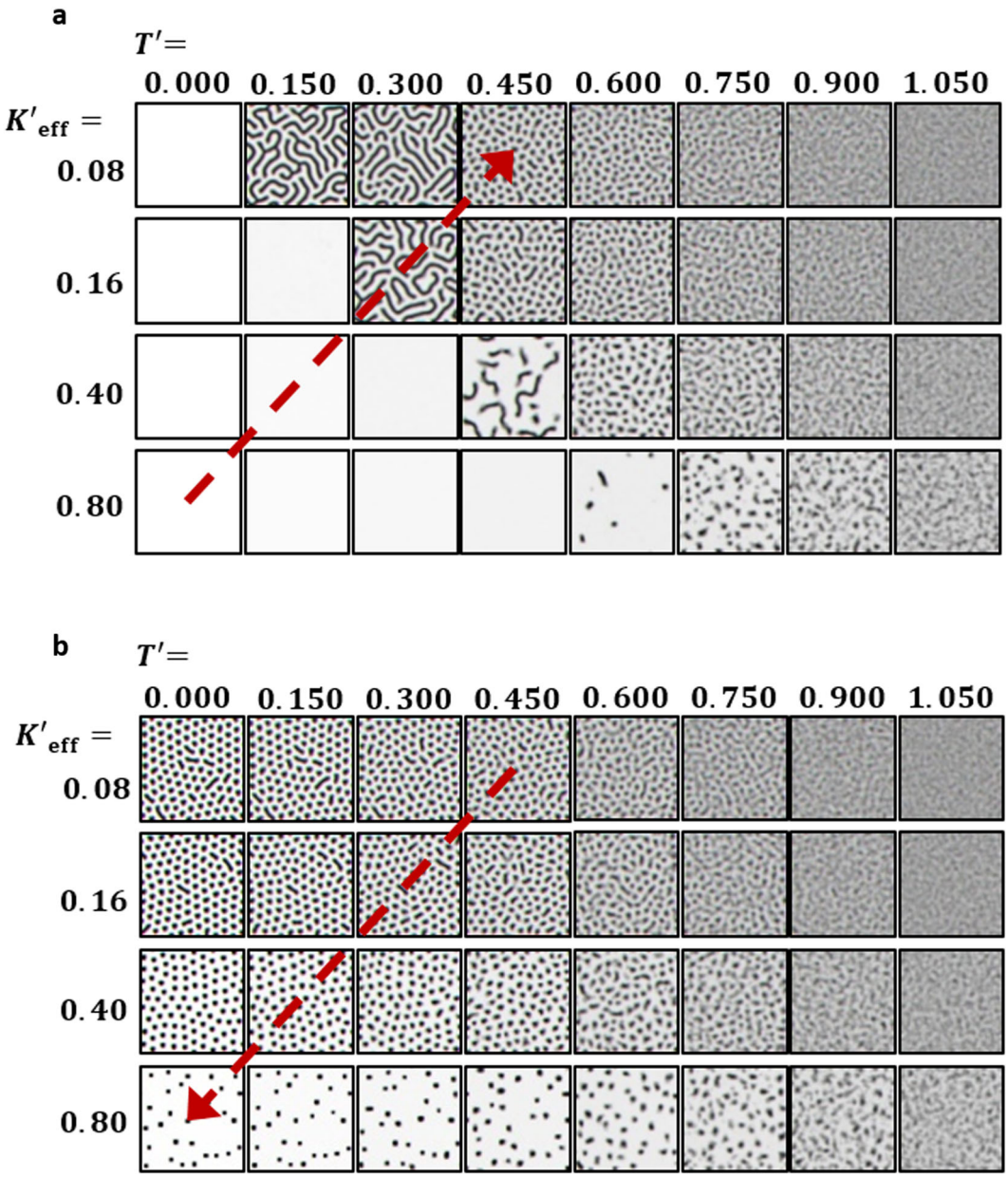

Fig. 3 Monte Carlo simulation of the temperature-dependent changes in the magnetic domain phase. The spin configurations are obtained using Eq. (1) and Eq. (2) in "Materials and methods", with the Hamiltonian parameters fixed to $|\overrightarrow{DM}_{ij}|/J = 0.3$, $D_{dip}/J = 0.2$, $|\vec{h}_{ext}|/J = 0.2$. **a**, **b** The magnetic domain phase evolution during the temperature increase (**a**) and decrease (**b**) process at four representative K'_{eff} values ($K'_{eff} \equiv K_{eff}/J$ and $T' \equiv T/J$). Each row of domain images is obtained in succession from left to right for **a** and from *right to left* for **b**. The experimentally observed magnetic domain evolution in Fig. 2 is reproduced along the red dotted lines, considering the observed temperature-dependent change in K'_{eff} (Fig. 1d).

(Fig. 2b), skyrmions appear in the temperature range of 733–323 K, agreeing with the simulations. From the excellent qualitative agreement between the experiments and simulations, we can conclude that the Néel-type skyrmions are the ground-state magnetic domains in a wide temperature range in this magnetic multilayer system.

Magnetic field dependence of the magnetic domain phase

To investigate the field-dependent magnetic domain phase evolution, the domain structures are observed while the external out-of-plane magnetic field is swept at a fixed sample temperature of 713 K. The stripe-to-skyrmion phase transition is observed as the out-of-plane magnetic field is increased from 0 to 28 mT (Fig. 4a), and the

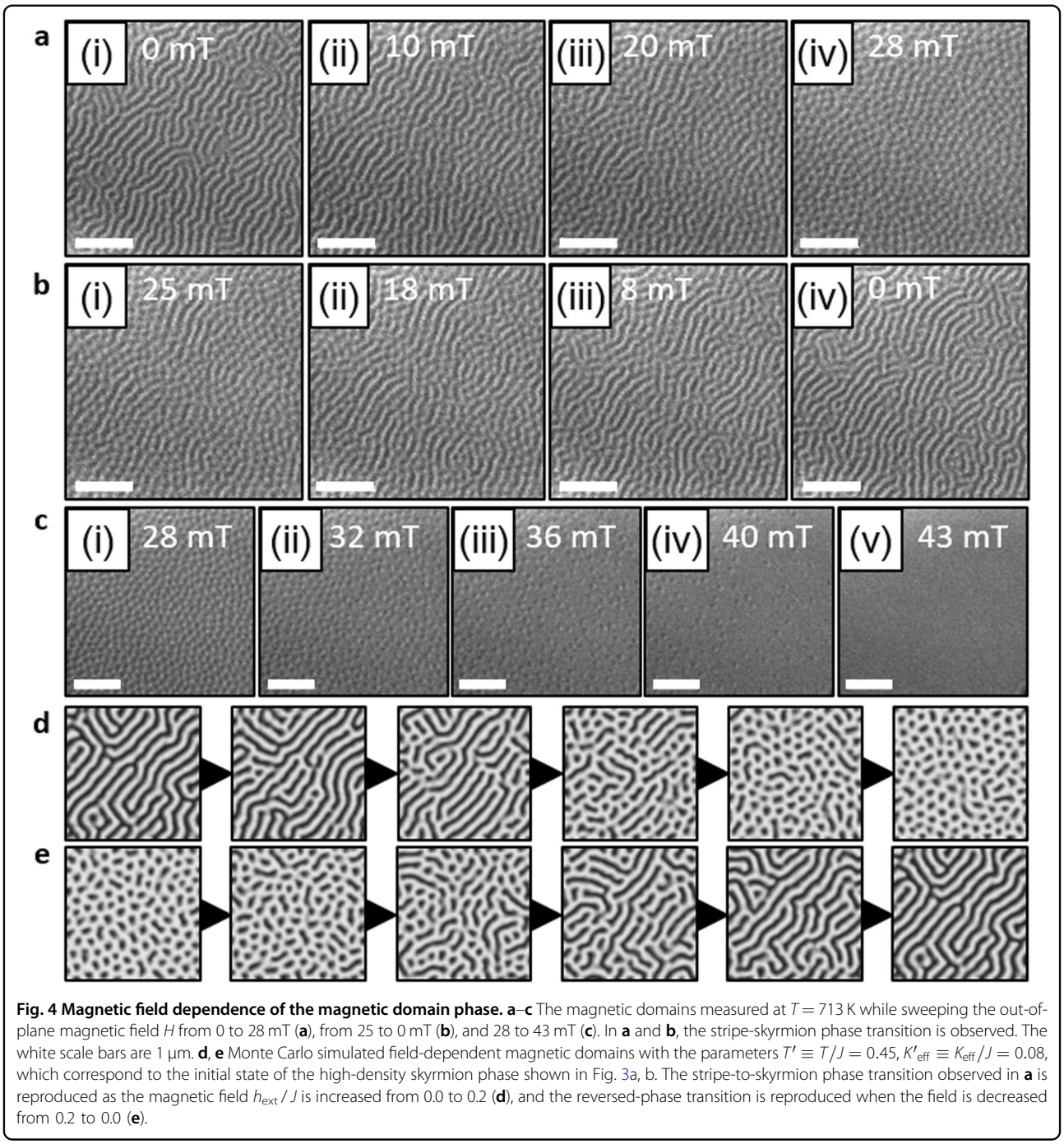

Fig. 4 Magnetic field dependence of the magnetic domain phase. a–**c** The magnetic domains measured at $T = 713$ K while sweeping the out-of-plane magnetic field H from 0 to 28 mT (**a**), from 25 to 0 mT (**b**), and 28 to 43 mT (**c**). In **a** and **b**, the stripe-skyrmion phase transition is observed. The white scale bars are 1 μm. **d**, **e** Monte Carlo simulated field-dependent magnetic domains with the parameters $T' \equiv T/J = 0.45$, $K'_{\mathrm{eff}} \equiv K_{\mathrm{eff}}/J = 0.08$, which correspond to the initial state of the high-density skyrmion phase shown in Fig. 3a, b. The stripe-to-skyrmion phase transition observed in **a** is reproduced as the magnetic field h_{ext}/J is increased from 0.0 to 0.2 (**d**), and the reversed-phase transition is reproduced when the field is decreased from 0.2 to 0.0 (**e**).

reversed-phase transition is observed as the field is decreased back to 0 mT (Fig. 4b). At a higher out-of-plane magnetic field, the free energy of the multiskyrmion state is lower than that of the stripe domain due to field-driven out-of-plane symmetry breaking[30,40], which leads to this reversible field-driven stripe-skyrmion phase transition. When the magnetic field is further increased to 43 mT, the high-density skyrmion phase is fully saturated into an out-of-plane single domain (Fig. 4c). The observed stripe-skyrmion phase transition process due to the external magnetic field is confirmed by micromagnetic simulations (Fig. 4d, e). In contrast to the temperature hysteresis behavior of the magnetic domain phase due to the temperature dependence of the magnetic anisotropy, the field-driven stripe-skyrmion phase transition is fully reversible in both experiments and simulations. This is

expected since the magnetic anisotropy does not change with the magnetic field.

Discussions and summary

Generally, the ground-state domain phase of magnetic materials is determined by various material parameters in the magnetic Hamiltonian, such as the magnetic anisotropy, magnetization, dipolar interaction, and DMI. The LTEM images and Monte Carlo simulations in this investigation show that with the careful selection of the magnetic anisotropy and magnetization (via magnetic field), a high-density Néel-type skyrmion phase can be stabilized in a wide temperature range in a magnetic multilayer system. In thin film systems, it is well known that the magnetic anisotropy and magnetization can be controlled systematically by the film thickness. Thus, our work suggests that with subtle tuning of the material properties (e.g., film thickness), multilayer-based skyrmionic devices can be designed to be employed at the preferred operating temperatures. While the high-density skyrmion phase is observed in the temperature range of $T = 423–733\,\mathrm{K}$ (150–460 °C) in our measurements, the Monte Carlo simulations in this study suggest that high-density skyrmion phases stabilized at lower or higher temperature ranges could be achievable through simultaneous tuning of the various material parameters (anisotropy, magnetization, etc.). In our Pt/Co/Ru/Pt/CoFeB/Ru multilayer structure, this is quite possible by adjusting both the Co and the CoFeB thicknesses and the ratio between the two.

In summary, we experimentally observe a high-density homochiral Néel-type skyrmion phase in a Pt/Co/Ru/Pt/CoFeB/Ru magnetic multilayer system that is stable at high temperature. The domain phase can be changed to a high-density skyrmion phase, an isolated skyrmion phase, or a stripe domain phase by controlling the magnetic field and temperature. Micromagnetic simulations confirm that domain phases, including the high-density skyrmion phase, can appear with the tuning of the magnetic anisotropy, magnetic field, and temperature. The existence of a high-density skyrmion phase at high temperature demonstrates the thermal stability of this magnetic domain phase. Moreover, considering that some electronic applications require operating temperatures up to 150 °C and possibly beyond[29], a spin information device utilizing the high-density skyrmion phase observed in a wide temperature range should provide an excellent alternative.

Acknowledgements

This work was mainly supported by the KIST Institutional Program (2E30600), the National Research Council of Science and Technology (NST) grant by the Ministry of Science and ICT (MSIT) (Grant No. CAP-16-01-KIST), the Basic Science Research Program through the National Research Foundation of Korea (NRF) funded by the Ministry of Education (NRF-2019R1A6A3A01091209), and the NRF funded by the MSIT (NRF-2020R1A5A1104591). J.J. and J.K. were supported by the Basic Science Research Program through the NRF funded by the MSIT (NRF-2017R1A2B4012482 and 2016K1A4A01922028) and the POSCO Green Science program. H.J.C. was supported by the Basic Science Research Program through the NRF funded by the MSIT (NRF-2017R1A2B2012514) and the KIST Institutional Program (2V06290). C.W. was supported by the NRF funded by the MSIT (NRF-2018R1D1A1B07047114).

Author details

[1]Center for Spintronics, Korea Institute of Science and Technology, Seoul 02792, Republic of Korea. [2]Department of Physics, Pohang University of Science and Technology, Pohang 37673, Republic of Korea. [3]Advanced Analysis Center, Korea Institute of Science and Technology, Seoul 02792, Republic of Korea. [4]Center for Research Equipment, Division of Scientific Instrumentation & Management, Korea Basic Science Institute, Daejeon 34133, Republic of Korea. [5]Center for Scientific Instrumentation, Division of Scientific Instrumentation & Management, Korea Basic Science Institute, Daejeon 34133, Republic of Korea. [6]Max Planck POSTECH Center for Complex Phase Materials, Pohang University of Science and Technology, Pohang 37673, Republic of Korea. [7]Department of Physics, Kyung Hee University, Seoul 02447, Republic of Korea. [8]Division of Nano & Information Technology, KIST School, University of Science and Technology, Seoul 02792, Republic of Korea

Conflict of interest

The authors declare that they have no conflict of interest.

Supplementary information is available for this paper at https://doi.org/10.1038/s41427-020-00270-z.

Received: 19 June 2020 Revised: 28 October 2020 Accepted: 2 November 2020.
Published online: 23 December 2020

References

1. Mühlbauer, S. et al. Skyrmion lattice in a chiral magnet. *Science* **323**, 915–919 (2009).
2. Yu, X. Z. et al. Real-space observation of a two-dimensional skyrmion crystal. *Nature* **465**, 901–904 (2010).
3. Heinze, S. et al. Spontaneous atomic-scale magnetic skyrmion lattice in two dimensions. *Nat. Phys.* **7**, 713–718 (2011).
4. Jonietz, F. et al. Spin transfer torques in MnSi at ultralow current densities. *Science* **330**, 1648–1651 (2010).
5. Yu, X. Z. et al. Skyrmion flow near room temperature in an ultralow current density. *Nat. Commun.* **3**, 988 (2012).
6. Romming, N. et al. Writing and deleting single magnetic skyrmions. *Science* **341**, 636–639 (2013).
7. Nagaosa, N. & Tokura, Y. Topological properties and dynamics of magnetic skyrmions. *Nat. Nanotechnol.* **8**, 899–911 (2013).
8. Fert, A., Cros, V. & Sampaio, J. Skyrmions on the track. *Nat. Nanotechnol.* **8**, 152–156 (2013).
9. Wang, K., Zhang, X. & Zhao, W. Skyrmion-electronics: an overview and outlook. *Proc. IEEE* **104**, 2040–2061 (2016).
10. Woo, S. et al. Deterministic creation and deletion of a single magnetic skyrmion observed by direct time-resolved X-ray microscopy. *Nat. Electron.* **1**, 288–296 (2018).
11. Jiang, W. et al. Blowing magnetic skyrmion bubbles. *Science* **349**, 283–286 (2015).
12. Woo, S. et al. Observation of room-temperature magnetic skyrmions and their current-driven dynamics in ultrathin metallic ferromagnets. *Nat. Mater.* **15**, 501–506 (2016).
13. Moreau-Luchaire, C. et al. Additive interfacial chiral interaction in multilayers for stabilization of small individual skyrmions at room temperature. *Nat. Nanotechnol.* **11**, 444–448 (2016).
14. Boulle, O. et al. Room-temperature chiral magnetic skyrmions in ultrathin magnetic nanostructures. *Nat. Nanotechnol.* **11**, 449–454 (2016).
15. Soumyanarayanan, A. et al. Tunable room-temperature magnetic skyrmions in Ir/Fe/Co/Pt multilayers. *Nat. Mater.* **16**, 898–904 (2017).

16. Legrand, W. et al. Room-temperature current-induced generation and motion of sub-100 nm skyrmions. *Nano Lett.* **17**, 2703–2712 (2017).
17. Hrabec, A. et al. Current-induced skyrmion generation and dynamics in symmetric bilayers. *Nat. Commun.* **8**, 15765 (2017).
18. Woo, S. et al. Current-driven dynamics and inhibition of the skyrmion Hall effect of ferrimagnetic skyrmions in GdFeCo films. *Nat. Commun.* **9**, 959 (2018).
19. Emori, S. et al. Current-driven dynamics of chiral ferromagnetic domain walls. *Nat. Mater.* **12**, 611–616 (2013).
20. Hsu, P.-J. et al. Electric-field-driven switching of individual magnetic skyrmions. *Nat. Nanotechnol.* **12**, 123–126 (2017).
21. Yu, G. et al. Room-temperature creation and spin–orbit torque manipulation of skyrmions in thin films with engineered asymmetry. *Nano Lett.* **16**, 1981–1988 (2016).
22. Büttner, F. et al. Field-free deterministic ultrafast creation of magnetic skyrmions by spin–orbit torques. *Nat. Nanotechnol.* **12**, 1040–1044 (2017).
23. Büttner, F. et al. Dynamics and inertia of skyrmionic spin structures. *Nat. Phys.* **11**, 225–228 (2015).
24. Woo, S. et al. Spin–orbit torque-driven skyrmion dynamics revealed by time-resolved X-ray microscopy. *Nat. Commun.* **8**, 15573 (2017).
25. Pinna, D. et al. Skyrmion gas manipulation for probabilistic computing. *Phys. Rev. Appl.* **9**, 064018 (2018).
26. Bourianoff, G., Pinna, D., Sitte, M. & Everschor-Sitte, K. Potential implementation of reservoir computing models based on magnetic skyrmions. *AIP Adv.* **8**, 055602 (2018).
27. Prychynenko, D. et al. Magnetic skyrmion as a nonlinear resistive element: a potential building block for reservoir computing. *Phys. Rev. Appl.* **9**, 014034 (2018).
28. Qin, Z. et al. Stabilization and reversal of skyrmion lattice in Ta/CoFeB/MgO multilayers. *ACS Appl. Mater. Interfaces* **10**, 36556–36563 (2018).
29. Iwata-Harms, J. M. et al. High-temperature thermal stability driven by magnetization dilution in CoFeB free layers for spin-transfer-torque magnetic random access memory. *Sci. Rep.* **8**, 14409 (2018).
30. Kwon, H. Y., Bu, K. M., Wu, Y. Z. & Won, C. Effect of anisotropy and dipole interaction on long-range order magnetic structures generated by Dzyaloshinskii-Moriya interaction. *J. Magn. Magn. Mater.* **324**, 2171–2176 (2012).
31. Kwon, H. Y. et al. A study of the stripe domain phase at the spin reorientation transition of two-dimensional magnetic system. *J. Magn. Magn. Mater.* **322**, 2742–2748 (2010).
32. Yafet, Y. & Gyorgy, E. M. Ferromagnetic strip domains in an atomic monolayer. *Phys. Rev. B* **38**, 9145–9151 (1988).
33. Seok, J. H. et al. In-plane spin reorientation transition in a two-dimensional ferromagnetic /antiferromagnetic system studied using Monte Carlo simulations. *Phys. Rev. B* **80**, 174407 (2009).
34. Huang, S. Y. et al. Transport magnetic proximity effects in platinum. *Phys. Rev. Lett.* **109**, 107204 (2012).
35. Lu, Y. M. et al. Pt magnetic polarization on $Y_3Fe_5O_{12}$ and magnetotransport characteristics. *Phys. Rev. Lett.* **110**, 147207 (2013).
36. Parkin, S. S. P., More, N. & Roche, K. P. Oscillations in exchange coupling and magnetoresistance in metallic superlattice structures: Co/Ru, Co/Cr, and Fe/Cr. *Phys. Rev. Lett.* **64**, 2304–2307 (1990).
37. Benitez, M. J. et al. Magnetic microscopy and topological stability of homochiral Néel domain walls in a Pt/Co/AlO_x trilayer. *Nat. Commun.* **6**, 8957 (2015).
38. Pollard, S. D. et al. Observation of stable Néel skyrmions in cobalt/palladium multilayers with Lorentz transmission electron microscopy. *Nat. Commun.* **8**, 14761 (2017).
39. Zhou, Y., Mansell, R., Valencia, S., Kronast, F. & van Dijken, S. Temperature dependence of the Dzyaloshinskii-Moriya interaction in ultrathin films. *Phys. Rev. B* **101**, 054433 (2020).
40. Buhrandt, S. & Fritz, L. Skyrmion lattice phase in three-dimensional chiral magnets from Monte Carlo simulations. *Phys. Rev. B* **88**, 195137 (2013).